Chapter

Synthesis of MCM-41/ZIF-67 Composite for Enhanced Adsorptive Removal of Methyl Orange in Aqueous Solution

Ratna Ediati, Pramita Elfianuar, Eko Santoso,
Dety Oktavia Sulistiono and Muhammad Nadjib

Abstract

ZIF-67 and MCM-41/ZIF-67 composites were successfully synthesized with water solvent at room temperature. The amounts of MCM-41 added during synthesis were varied at 2.5, 5 and 10 (%w/w) toward the amount of ZIF-67, and the obtained solids were denoted as MC (2.5)/ZIF-67, MC (5)/ZIF-67, and MC (10)/ZIF-67, respectively. The X-ray diffraction (XRD) patterns of ZIF-67 and the composites showed characteristic peaks at 2θ of 7.32, 10.36, 12.69, 14.66, and 16.40°, similar to that of reported ZIF-67. The Fourier transform infra-red (FT-IR) spectra of all solids showed absorption bands at the same wavenumbers as reported for ZIF-67. The results of surface morphology analysis using scanning electron microscope (SEM) have shown that ZIF-67 and the composites have a cube shape, which is characteristic for the ZIF-67 standard. N_2 adsorption-desorption data showed that the specific surface area of ZIF-67 and MC (5)/ZIF-67 were 1079.2 and 1011.2 m^2/g, respectively, lower than that of MC (10)/ZIF-67 (1250.6 m^2/g). However, results of thermal gravimetric analysis (TGA) showed that the thermal stability of MC (10)/ZIF-67 reached 357°C, higher than that of ZIF-67 (325°C). Performance of the composites as adsorbent of methyl orange (MO) in aqueous solution showed that the MC (5)/ZIF-67 had the highest adsorption capacity of 167.635 mg/g, and followed the pseudosecond-order adsorption kinetics and Langmuir isothermal adsorption.

Keywords: ZIF-67, composite, MCM-41/ZIF-67, adsorption, methyl orange

1. Introduction

Organic dyes are pollutants that can provide toxic effects on microbial populations and can be toxic or carcinogenic to organisms and mammals [1]. Azo dyes are a group of synthetic organic dyes, which are most widely used in the textile, cosmetics, and food coloring industries, so they are found in industrial waste water. The release of waste water containing dyes, with different chemical compositions and toxicity, into waterways can cause environmental damage [2]. Methyl orange (MO) is one of the cationic dyes, which are widely used in the coloring industry. If the MO concentration in wastewater reaches 500 ppm, it can cause serious health

problems, such as tachycardia, vomiting, cyanosis, jaundice, quadriplegia, and tissue necrosis. Therefore, removing MO in wastewater is needed to avoid the negative effects that arise [3–5].

Several methods have been reported to remove organic dyes in water, such as adsorption with solid materials [6], chemical and biological degradation [7, 8], electrochemical degradation [9], and ozonation [10]. Adsorption, however, is considered as a simple and effective method. The adsorbents used, such as activated carbon, agricultural waste, and chitosan [11], have shown low adsorption capacity and selectivity [12].

Metal organic frameworks (MOF) are a new class of nanoporous crystalline materials consisting of metal ions or clusters that are interconnected with organic ligands and described as materials with microstructure (pore size < 2 nm), adjustable pore size, high surface area (up to 5900 m^2/g), and high pore volume (up to 2 cm^3/g) [13–15]. With the advantages, MOF has been considered as a potential material for various applications, including gas storage, separation, adsorption, drug delivery, and catalysts [15]. As an adsorbent, MOF has been widely used to remove toxic metals and organic pollutants from aqueous solutions [16].

Zeolitic imidazolate frameworks (ZIF) are parts of MOF, composed of tetrahedral metal ions such as Zn^{2+} or Co^{2+}, which are bridged by imidazolate ligands [17, 18]. ZIF-67 (Co(Hmim)$_2$), with a sodalite (SOD) topology [18], has been evaluated for its performance as an adsorbent in an aqueous environment and shows a high adsorption capacity against several pollutants including azo dyes [12, 19]. In the adsorption process, the pore size of adsorbent is very influential. MOF with pore size of less than 2 nm (microporous) may cause diffusion problems toward large molecules. Mesoporous silica such as MCM-41, MCM-48, and SBA-15 have been reported as supports in MOF synthesis, as an effort to increase pore size of MOF and to reduce diffusion problems when used as adsorbents. Furthermore, mesoporous silica also has high thermal stability, surface area, and porosity [20, 21].

Based on the description above, in this study, removal of MO in aqueous solution was carried out using ZIF-67 and MCM-41/ZIF-67 composites. ZIF-67 and the composites were synthesized following the method reported by Gross et al. with a slight modification [22]. The experiments were carried out at room temperature with CoCl$_2$·6H$_2$O as a metal source and 2-methylimidazole as a ligand in aqueous solution. A certain amount of MCM-41 was added directly into the reaction mixture.

2. Experimental

2.1 Materials

Materials used in this study were cobalt chlorida hexahydrate (CoCl$_2$.6H$_2$O, Sigma Aldrich, 99%), 2-methylimidazole (C$_4$H$_6$N$_2$, Sigma Aldrich, 99%), deionized water, triethylamine (TEA), methanol (MeOH, Merck 99.8%), and methyl orange (Sigma Aldrich, 85%). Mesoporous silica (MCM-41) was synthesized using a procedure reported by Badamali et al. [23].

2.2 Synthesis of ZIF-67 and composite MCM-41/ZIF-67

ZIF-67 and MCM-41/ZIF-67 composites were synthesized with a molar ratio of metal:ligand of 1:11.6. The synthesis of ZIF-67 was begun by dissolving 6.09 g of 2-methylimidazole (MeIM) in 13.5 mL deionized water. Triethylamine (TEA) added was 0.5 mL and the amount of MCM-41 added was varied at 2.5, 5 and 10 w/w% toward the amount of the obtained ZIF-67. Then, CoCl$_2$·6H$_2$O solution was made

by dissolving 1.52 g of $CoCl_2 \cdot 6H_2O$ in 10 mL deionized water. $CoCl_2 \cdot 6H_2O$ solution was mixed with 2-methylimidazole solution in a vial bottle and stirred for 20 min. Furthermore, the reaction mixture was centrifuged at 3000 rpm for 30 min. The obtained solids were washed with deionized water, followed by washing with methanol. Finally, the solids were dried in an oven at a temperature of 120°C for 16 hours.

2.3 Characterization ZIF-67 and MCM-41/ZIF-67 composites

The crystallinity of ZIF-67 and MCM-41/ZIF-67 composites were determined by XRD with CuKα radiation (λ = 1.5406 Å), with 40 kV accelerated voltage, and a current of 30 mA. The 2θ angle was recorded from 3 until 50°. Analysis of the existence of functional groups on ZIF-67 and MCM-41/ZIF-67 composites was carried out by FTIR spectrophotometer at wavenumbers of 4000–400 cm^{-1}. Analysis by scanning electron microscope (SEM) has been done to determine the surface morphology of synthesized material. TEM images were obtained using a JEOL JEM1400 transmission electron microscope at an accelerating voltage of 200 kV. Measurement of surface area and pore size distribution of the materials were carried out using surface area analyzer based on adsorption-desorption isotherm using nitrogen gas, and the samples were degassed at 150°C for 5 hours (3×10^{-3} Torr) before being analyzed. Thermogravimetric analysis (TGA) has been used to determine the thermal stability, and the samples were heated from temperature of 35–700°C with an air gas flow.

2.4 Adsorption experiment

Methyl orange (MO) adsorption test on the effect of contact time was carried out using 10 mg of adsorbent in 100 mg/L of MO solution. The mixture was stirred at 300 rpm for 5 until 40 min. In addition, the adsorption test was also carried out on the effect of the initial concentration and concentration of MO was varied from 50 to 330 mg/L. After adsorption process, the solution was centrifuged at a rate of 3500 rpm for 10 min to separate the adsorbent from the solution. Concentration of MO was measured using a UV-Vis spectrophotometer at the maximum wavelength. Adsorption capacities of adsorbent and %removal of MO were calculated using the formula:

$$Q_e = \frac{(C_o - C_e) \times V}{W} \qquad (1)$$

$$\%Removal = \frac{C_0 - C_e}{C_o} \times 100 \qquad (2)$$

where C_o and C_e are initial and equilibrium concentrations of MO in mg/L, W is the mass of adsorbent in g, and V is the volume of solution in mL.

3. Result and discussion

3.1 Characterization of materials

The effect of the addition of MCM-41 on characteristic of the obtained MCM-41/ZIF-67 composites has been determined from the results of characterization using XRD, FTIR, SEM-EDX, nitrogen adsorption-desorption, and TGA. The XRD patterns of ZIF-67 and MCM-41/ZIF-67 composites are shown in **Figure 1**. As can be seen, the characteristic peaks appear at 2θ of 7.32, 10.36, 12.69, 14.66, and 16.40°,
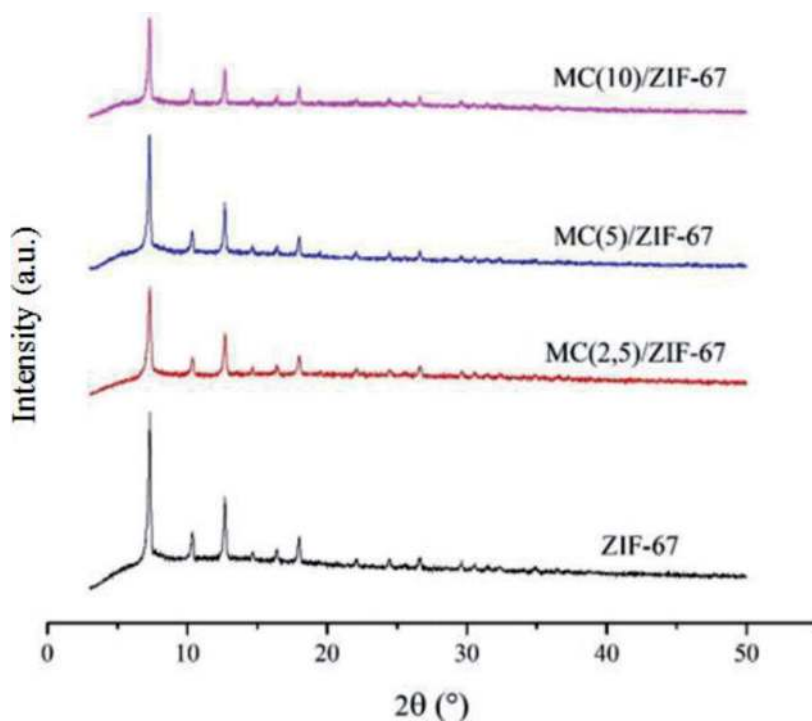
Figure 1.
XRD pattern of ZIF-67 and MCM-41/ZIF-67 composites.

respectively, which are in accordance with the results of previous studies [22]. Likewise, the XRD patterns of the MCM-41/ZIF-67 composites have shown the same pattern as pure ZIF-67. The addition of MCM-41 during the ZIF-67 synthesis, however, has resulted in a reduction in crystallinity of the obtained composites, which may be attributed to amorphous properties of mesoporous silica [24].

FT-IR analysis has been carried out to identify the functional groups of the obtained materials, and the results are shown in **Figure 2**. Each sample exhibit the presence of a sharp absorption band at a wavenumber of 423 cm^{-1}, due to the Co—N stretching vibration, indicating a bond between Co and N of the 2-methylimidazole ligand [25]. An absorption band at 693 cm^{-1} may be attributed to the bending vibration of the ring 2-metilimidazole [26]. Absorption peaks at wavenumbers of 755 and 1577 cm^{-1} may be resulted from out-of-plane vibrations and stretching vibrations of C $=$ N in 2-methylimidazole ligands. The occurrence of C—N bending vibration has been identified from the appearance of a peak at wavenumber of 992 cm^{-1}, while stretching vibration from C—N is identified at wavenumber 1141 cm^{-1}. Absorption bands at wavenumbers 2926 and 3134 cm^{-1} appear due to stretching vibration of C—H sp^3 aromatic ring on 2-methylimidazole and stretching vibration of C—H sp^2 on aliphatic hydrocarbon chains [25]. The characteristic peak of MCM-41 that appears at wavenumber of 1050 cm^{-1}, as a result of Si—O—Si asymmetric vibration, is seen in the MC(5)/ZIF-67 composite spectrum and appears more pronounced in the MC(10)/ZIF-67 composite. This observation has indicated the existence of MCM-41 in the composite.

Surface morphology of ZIF-67, as is shown in **Figure 3(a)**, has a cubic shape, similar to that reported by Qian et al. [18]. Likewise, the MC(10)/ZIF-67 composite also has a uniform surface morphology, as is shown in **Figure 3(b)**. The results of SEM showed that the presence of mesoporous silica resulted in the increase in particle size, while the cube shape and more uniform surface morphology remained unchanged. The SEM images may indicate that the growth of ZIF-67 has taken place
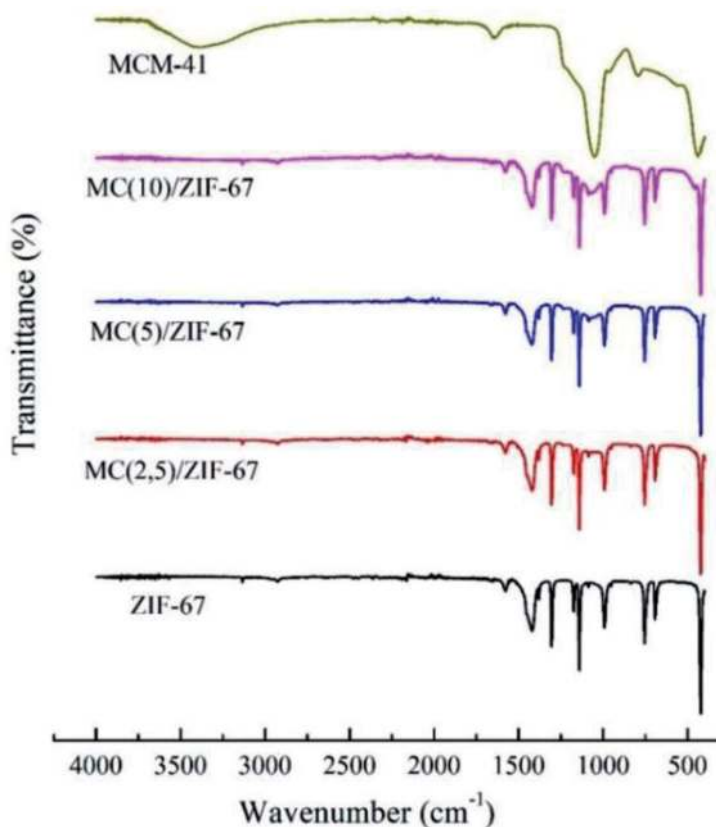
4

Figure 2.
FT-IR spectra of ZIF-67 and the composites.

inside the pores as well as on the surface of mesoporous silica. The phenomenon is reinforced by TEM image of the MC(10)/ZIF-67 composite, in which the characteristic hexagonal pore shape of MCM-41 is not seen any more in **Figure 3(c)**.

Nitrogen adsorption-desorption isotherms and pore size distributions of ZIF-8, and the composites are presented in **Figure 4(a)** and **(b)**, respectively, and the results of BET surface area and pore size are summarized in **Table 1**.

As shown in **Figure 4(a)**, type I isotherm adsorption curves of ZIF-67 and the composites have indicated that adsorption occurred in micropores of the samples that have high surface area. At a relatively higher pressure ($P/P_0 = 0.85–1$), the amount of gas absorbed increased and a narrow vertical hysteresis loop was observed on all samples, which may be due to the presence of interparticle mesoporous. Based on the BET equation, the highest surface area was observed for
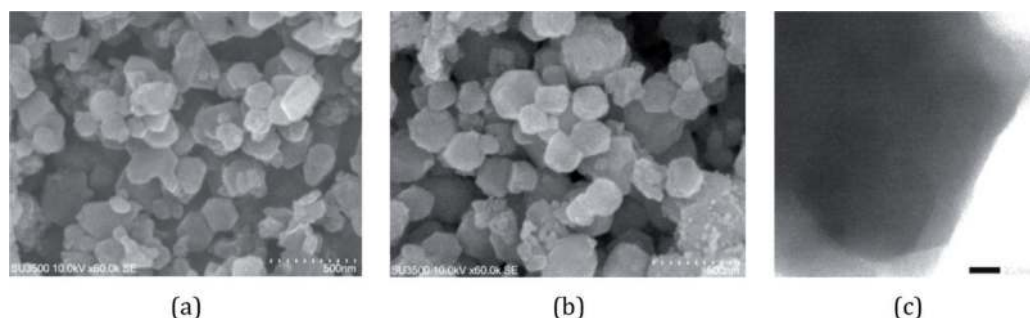

Figure 3.
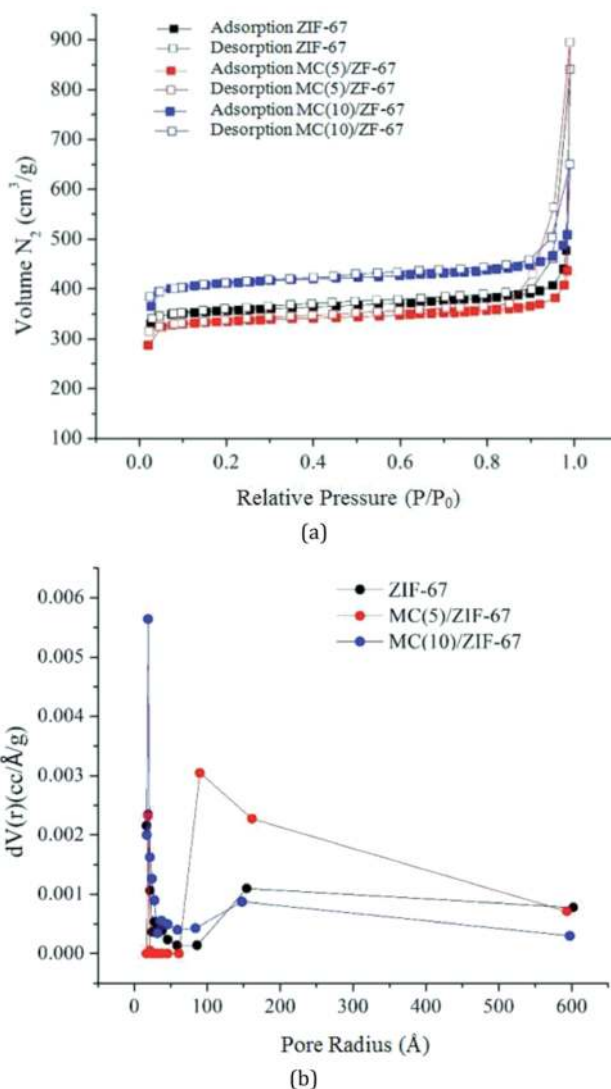*SEM image of (a) ZIF-67 (b) MC (10)/ZIF-67 (c) and TEM image of MC (10)/ZIF-67.*

Figure 4.
(a) N₂ adsorption-desorption isotherm and (b) pore distribution of ZIF-67 and the composites.

MC(10)/ZIF-67 (1250.6 m²/g). The high surface area may result from the formation of ZIF-8 particles inside the MCM-41 mesopores so as to produce new micropores with high surface area [27]. The pore distribution curves of ZIF-67 and the composites based on the BJH method are shown in **Figure 4b**, in which microporous and mesoporous distributions have been observed (**Table 1**). It can be concluded that the addition of mesoporous silica into the ZIF-8 synthesis results in the increase in the pore volume and pore diameter of the obtained composites (**Figure 4b**).

The results of TGA, as is shown in **Figure 5**, confirmed two-stage process of decomposition of ZIF-67 and MC(10)/ZIF-67 composite.

At a temperature range of 35–325°C, a mass decrease of 7.68% was observed, as a result of the loss of guest molecules of solvent or ligands that occupied the pores or surface of the samples [18]. Furthermore, a sharp decrease of 60.05% mass was observed in the temperature range of 325–429°C, which considered as decomposition of 2-methylimidazole ligand and damage of ZIF-67 structure. In addition, it can be seen in **Figure 5** that the thermal stability of the MC(10)/ZIF-67 was slightly higher than that of ZIF-67. The observation was in accordance with the result reported by Bhatt et al. [28]. Also, higher remaining mass of the composite as compared to the ZIF-67 was due to presence of SiO_2 from the MCM-41 added.

Materials	S_{BET}^{a} (m^2/g)	V_{meso}^{b} (cm^3/g)	V_{micro}^{c} (cm^3/g)	D^d (nm)
MCM-41	887.5	0.33	0.33	3.81
ZIF-67	1079.2	0.83	0.47	4.82
MC(5)/ZIF-67	1011.2	0.98	0.39	5.47
MC(10)/ZIF-67	1250.6	0.50	0.50	3.21

^{a}*BET surface area.*

^{b}*Mesopore volume calculated using BJH method.*

^{c}*Micropore volume calculated using t-plot method.*

^{d}*Average pore diameter.*

Table 1.
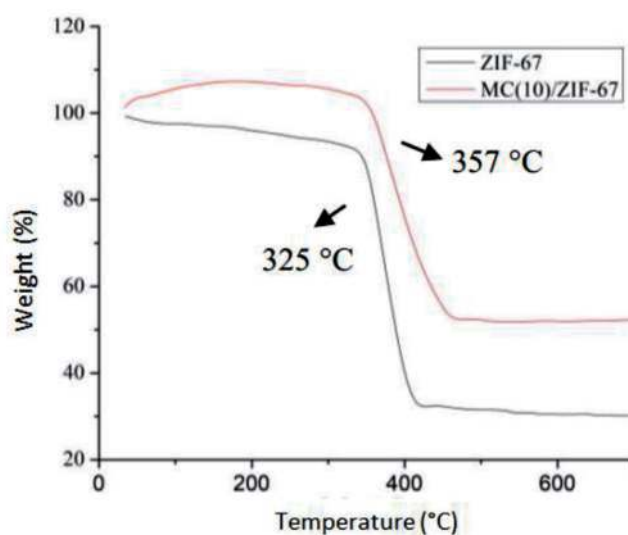*Summary of the textural properties of the synthesized material at different addition of MCM-41.*

Figure 5.
Thermogravimetric profiles of ZIF-7 and MC(10)/ZIF-67 composite.

3.2 Adsorption kinetic studies

Kinetic study of MO adsorption was carried out using 20 mL of MO solution with a concentration of 100 mg/L. The contact times were varied in the range of 5–40 min, while the weight of adsorbent was 10 mg. The effect of contact time on MO adsorption for ZIF-67, MC(5)/ZIF-67, and MC(10)/ZIF-67 materials is illustrated in **Figure 6**. It can be seen that adsorption capacities increased with the increase in contact time to reach a maximum value after 25 min, after which a more stable adsorption capacity was observed until 50 min. The results indicated that the empty space of pores and the surface of adsorbent have been completely filled with adsorbate [29].

The kinetics data were analyzed using pseudofirst-order and pseudosecond-order kinetic models using Eqs. (3) and (4).

$$Ln(Q_e - Q_t) = Ln\,Q_e - K_1 t \tag{3}$$

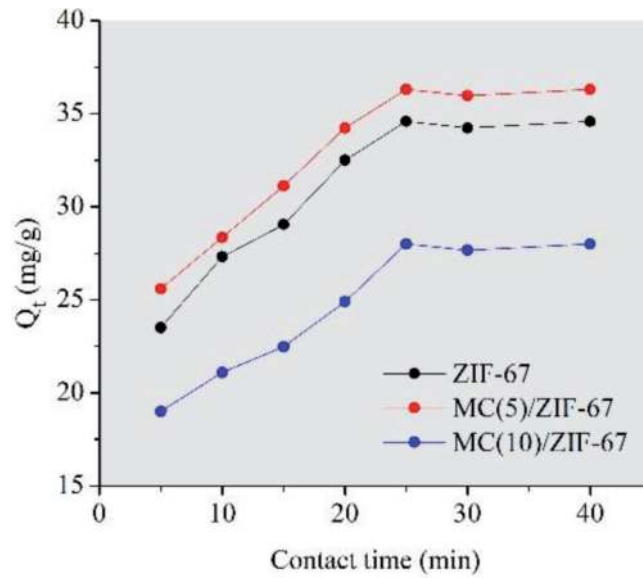$$\frac{t}{Q_t} = \frac{1}{K_2 Q_e^2} + \frac{t}{Q_e} \tag{4}$$

Figure 6.
Effect of contact time on MO adsorption.

Based on the calculation of adsorption kinetics with Eqs. (3) and (4), graph plots were performed on each of the adsorption kinetics models and the obtained graphs are shown in **Figure 7**. MO adsorption kinetics model of ZIF-67, MC(5)/ZIF-67, and MC(10)/ZIF-67 adsorbents were determined by comparing the R^2 values of each graph of the adsorption kinetics as shown in **Table 2**. It can be seen that correlation coefficient of the pseudosecond-order plot is higher than the pseudofirst-order plot. The results indicated that the mechanism of adsorption in all materials observed was as a result of chemisorption [30].

Adsorption of MO at different initial concentrations was carried out at the optimum contact time obtained of 25 min with MO concentration in the range of 50–330 mg/L. As is shown in **Figure 8**, the adsorption capacity increased with the increase in initial concentration of MO and the equilibrium of adsorption capacity was observed at an initial concentration of 285.20 mg/L. By further increasing the initial MO concentrations, a stable equilibrium adsorption capacity was obtained.
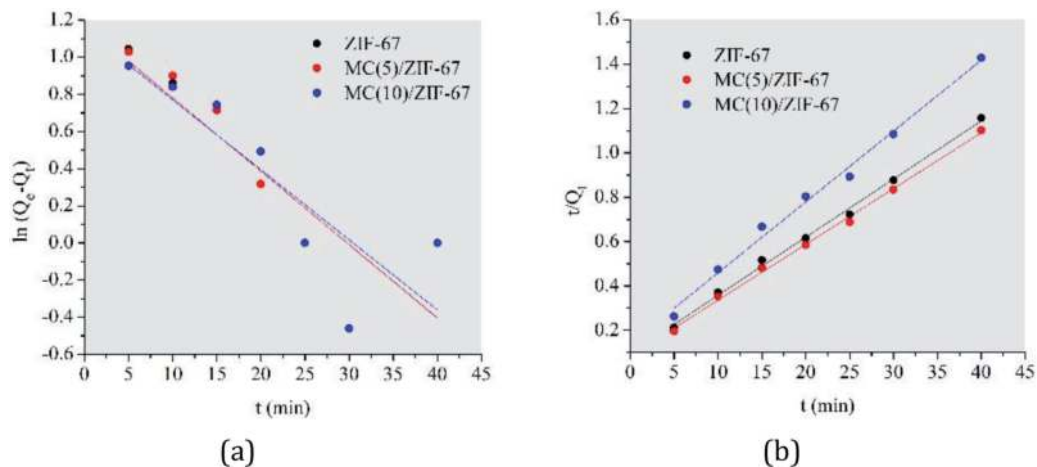

Figure 7.
Plots of (a) pseudofirst-order kinetics and (b) pseudosecond-order kinetics for the adsorption of MO.

Adsorbent	$Qe_{(exp)}$	Pseudofirst order			Pseudosecond order		
		$Qe_{(cal)}$	K_1	R^2	$Qe_{(cal)}$	K_2	R^2
ZIF-67	34.5782	3.2381	0.0395	0.7534	38.0228	0.00737	0.9967
MCM-41/ ZIF-67(5)	36.3071	3.2407	0.0395	0.7545	39.6825	0.00752	0.9970
MCM-41/ ZIF-67(10)	28.0083	3.1525	0.0377	0.7377	31.3480	0.00726	0.9923

Table 2.
Kinetic parameters and correlation coefficients for the pseudofirst-order and pseudosecond-order equations.

The MC(5)/ZIF-67 showed highest Q_e value of 167.64 mg/g, compared to other adsorbents. The results of adsorption studies have been in accordance with the results of N_2 adsorption-desorption analysis, in which the higher the pore size of the adsorbent, the higher is the adsorption capacity. The largest pore size of MC(5)/ZIF-67, as a result of adding 5%w/w mesoporous silica during the ZIF-67 synthesis, has improved its performance in MO adsorption [26]. The large pore size of the MC(5)/ZIF-67 allowed MO molecules to easily diffuse in to the pores and interacted electrostatically with cobalt ions from ZIF-67.

3.3 Isotherm adsorption

The study of adsorption isotherms was based on Langmuir and Freundlich isotherms models as calculated in Eqs. (5) and (6):

$$\frac{1}{Q_e} = \frac{1}{Q_m} + \frac{1}{Q_m \times K_L \times C_e} \qquad (5)$$

$$LnQ_e = LnK_F + \frac{1}{n}LnC_e \qquad (6)$$

Plots of adsorption isotherm obtained from the calculation are presented in **Figure 9**. The calculated correlation coefficient for each adsorbent used approaches
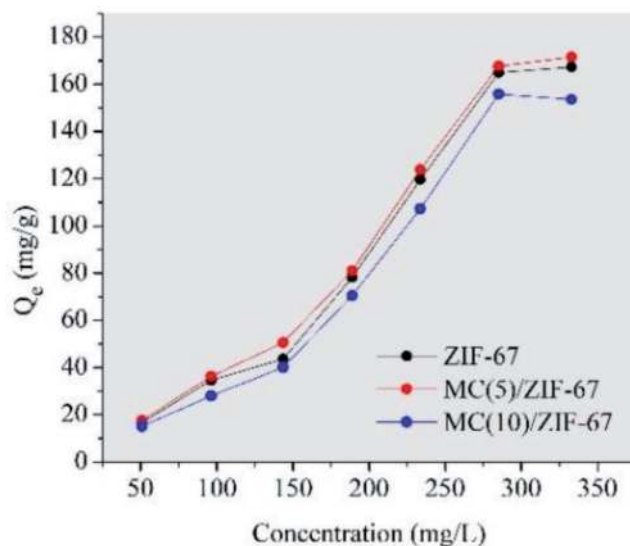

Figure 8.
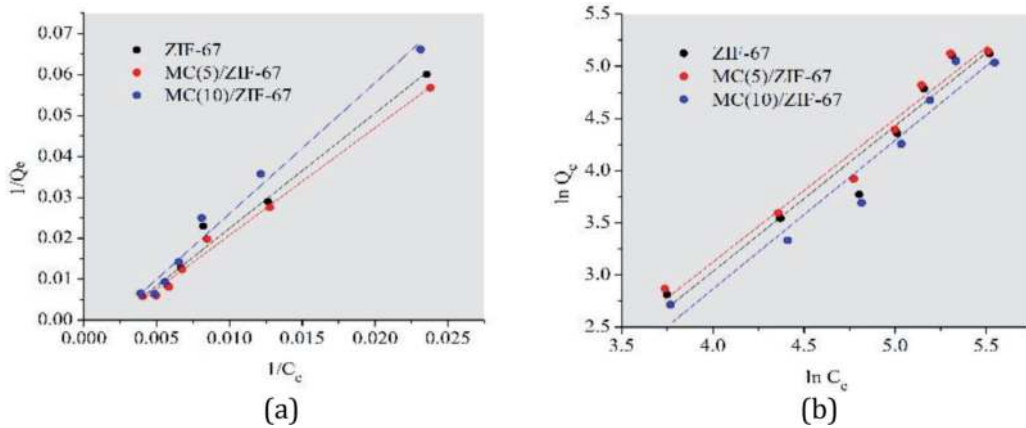*Effect of initial concentrations of MO.*

Figure 9.
Plots of (a) Langmuir and (b) Freundlich models of MO adsorption.

Adsorbent	Qe$_{(exp)}$	Langmuir			Freundlich		
		Q$_m$ (mg/g)	K$_L$ (L/mg)	R^2	K$_F$ (mg/g)	n	R^2
ZIF-67	164.877	175.439	0.0020	0.982	12.705	0.7172	0.946
MC(5)/ZIF-67	167.635	181.818	0.0021	0.992	10.578	0.7296	0.965
MC(10)/ZIF-67	155.878	166.667	0.0019	0.981	17.0134	0.7018	0.956

Table 3.
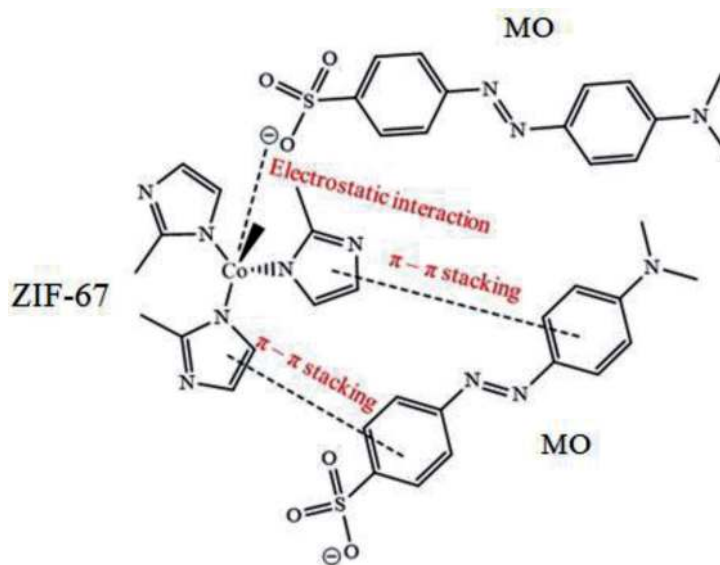*Langmuir and Freundlich isotherm parameters for the adsorption of MO.*

Figure 10.
Mechanism of MO adsorption to ZIF-67.

with the value of 1 in the Langmuir model (**Table 3**). These results indicated that the adsorption process occurred in accordance with the Langmuir adsorption isotherm model, which led to the assumption that adsorption occurred on a specific homogeneous surface of the adsorbent, which had the same energy for monolayer adsorption [31].

As an anionic dye, MO contains SO_3 group in its molecular structure. The adsorption of MO by ZIF-67 and MCM-41/ZIF-67 composites can occur as a result of the electrostatic interaction between the SO_3 group and the positive charge of cobalt ion from ZIF-67 [12]. In addition, the imidazole rings of ZIF-67 may interact with the benzene rings from MO molecules through π-π stacking [16, 19]. The molecular interaction of MO with ZIF-67 is illustrated in **Figure 10**.

4. Conclusions

ZIF-67 and MCM-41/ZIF-67 composites have been successfully synthesized at room temperature in aqueous solution with addition of TEA as a deprotonating agent. The results of characterization using XRD indicated that both ZIF-67 and composites exhibited the same diffractogram patterns, with characteristic peaks at 2θ of 7.32, 10.36, 12.69, 14.66, and 16.40°, similar to that of reported ZIF-67. In addition, the absorption bands of FTIR spectra of all composites appeared at the same wavenumber as observed for synthesized and the reported ZIF-67. SEM images showed similar cube shapes of surface morphology between ZIF-67 and MC(10)/ZIF-67 composites. The results of analysis by adsorption-desorption N_2 showed that the highest surface area of 1250.6 m^2/g was observed for MC(10)/ZIF-67. The highest adsorption capacity toward MO in aqueous solution of 167.6 mg/g was achieved by MC(5)/ZIF-67 adsorbent, and followed a pseudosecond-order adsorption kinetics and Langmuir adsorption isotherm.

Acknowledgements

Author details

Ratna Ediati*, Pramita Elfianuar, Eko Santoso, Dety Oktavia Sulistiono and Muhammad Nadjib
Department of Chemistry, Institut Teknologi Sepuluh Nopember (ITS), Surabaya, Indonesia

*Address all correspondence to: ratna.ediati@gmail.com

IntechOpen

References

[1] Chatterjee S, Lee DS, Lee MW, Woo SH. Congo red adsorption from aqueous solutions by using chitosan hydrogel beads impregnated with nonionic or anionic surfactant. Bioresource Technology. 2009;**100**:3862-3868. DOI: 10.1016/j.biortech.2009.03.023

[2] Shi L, Hu L, Zheng J, Zhang M, Xu J. Adsorptive removal of methylene blue from aqueous solution using a Ni-metal organic framework material. Journal of Dispersion Science and Technology. 2016;**37**:1226-1231. DOI: 10.1080/01932691.2015.1050731

[3] Chen S, Huang Y, Han X, Wu Z, Lai C, Wang J, et al. Simultaneous and efficient removal of Cr(VI) and methyl orange on LDHs decorated porous carbons. Chemical Engineering Journal. 2018. DOI: 10.1016/j.cej.2018.07.012

[4] Habiba AU, Siddique TA, Jia J, Lee L, Joo TC, Ang BC, et al. Adsorption study of methyl orange by chitosan/polyvinyl alcohol/zeolite electrospun composites nanofibrous membrane. Carbohydrate Polymers. 2018. DOI: 10.1016/j.carbpol.2018.02.081

[5] Gracia F, Lee AF, Mansoob M. Mechanothermal synthesis of Ag/TiO_2 for photocatalytic methyl orange degradation and hydrogen production. Process Safety and Environmental Protection. 2018. DOI: 10.1016/j.psep.2018.09.015

[6] Khan NA, Hasan Z, Jhung SH. Adsorptive removal of hazardous materials using metal-organic frameworks (MOFs): A review. Journal of Hazardous Materials. 2012:1-13. DOI: 10.1016/j.jhazmat.2012.11.011

[7] Houas A et al. Photocatalytic degradation pathway of methylene blue in water. Applied Catalysis B: Environmental. 2001;**31**:145-157. DOI: 10.1016/S0926-3373(00)00276-9

[8] Ayed L, Mahdhi A, Cheref A, Bakhrouf A. Decolorization and degradation of azo dye Methyl Red by an isolated *Sphingomonas paucimobilis*: Biotoxicity and metabolites characterization. Desalination. 2011;**274**:272-277. DOI: 10.1016/j.desal.2011.02.024

[9] Li SH, Zhao Y, Chu J, Li WW, Yu HQ, Liu G. Electrochemical degradation of methyl orange on Pt-Bi/C nanostructured electrode by a square-wave potential method. Electrochimica Acta. 2013;**92**:93-101. DOI: 10.1016/j.electacta.2013.01.012

[10] Bamperng S, Suwannachart T, Atchariyawut S, Jiraratananon R. Ozonation of dye wastewater by membrane contactor using PVDF and PTFE membranes. Separation and Purification Technology. 2010;**72**:186-193. DOI: 10.1016/j.seppur.2010.02.006

[11] Yang Y, Yan X, Hu X, Feng R, Zhou M. In-situ growth of ZIF-8 on layered double hydroxide: Effect of Zn/Al molar ratios on their structural, morphological and adsorption properties. Journal of Colloid and Interface Science. 2017;**505**:206-212. DOI: 10.1016/j.jcis.2017.05.100

[12] Zhang ZH, Zhang JL, Liu JM, Xiong ZH, Chen X. Selective and competitive adsorption of azo dyes on the metal–organic framework ZIF-67. Water, Air, and Soil Pollution. 2016;**227**. DOI: 10.1007/s11270-016-3166-7

[13] Khan NA, Jung BK, Hasan Z, Jhung SH. Adsorption and removal of phthalic acid and diethyl phthalate from water with zeolitic imidazolate and metal-organic frameworks. Journal of Hazardous Materials. 2015;**282**:194-200. DOI: 10.1016/j.jhazmat.2014.03.047

[14] Tan K, Zuluaga S, Gong Q, Canepa P, Wang H, Li J, et al. Water

reaction mechanism in metal organic frameworks with coordinatively unsaturated metal ions: MOF-74. Chemistry of Materials. 2014;**26**: 6886-6895. DOI: 10.1021/cm5038183

[15] Cho HY, Yang DA, Kim J, Jeong SY, Ahn WS. CO_2 adsorption and catalytic application of Co-MOF-74 synthesized by microwave heating. Catalysis Today. 2012;**185**:35-40. DOI: 10.1016/j. cattod.2011.08.019

[16] Hasan Z, Jhung SH. Removal of hazardous organics from water using metal-organic frameworks (MOFs): Plausible mechanisms for selective adsorptions. Journal of Hazardous Materials. 2015;**283**:329-339. DOI: 10.1016/j.jhazmat.2014.09.046

[17] Park KS, Ni Z, Côté AP, Choi JY, Huang R, Uribe-Romo FJ, et al. Exceptional chemical and thermal stability of zeolitic imidazolate frameworks. Proceedings of the National Academy of Sciences of the United States of America. 2006;**103**:10186-10191. DOI: 10.1073/ pnas.0602439103

[18] Qian J, Sun F, Qin L. Hydrothermal synthesis of zeolitic imidazolate framework-67 (ZIF-67) nanocrystals. Materials Letters. 2012;**82**:220-223. DOI: 10.1016/j.matlet.2012.05.077

[19] Lin KA, Chang H. Chemosphere ultra-high adsorption capacity of zeolitic imidazole framework-67 (ZIF-67) for removal of malachite green from water. Chemosphere. 2015;**67**:1-8. DOI: 10.1016/j.chemosphere.2015.01.041

[20] Kondo A, Takanashi S, Maeda K. New insight into mesoporous silica for nano metal-organic framework. Journal of Colloid and Interface Science. 2012. DOI: 10.1016/j.jcis.2012.06.040

[21] Zhao XS, Lu GQ. Modification of MCM-41 by surface silylation with trimethylchlorosilane and adsorption

study. The Journal of Physical Chemistry. B. 1998. DOI: 10.1021/jp972788m

[22] Gross AF, Sherman E, Vajo JJ. Aqueous room temperature synthesis of cobalt and zinc sodalite zeolitic imidizolate frameworks. Dalton Transactions. 2012;**41**:5458. DOI: 10.1039/c2dt30174a

[23] Badamali S, Sakthivel A, Selvam P. Influence of aluminium sources on the synthesis and catalytic activity of mesoporous AlMCM-41 molecular sieves. Catalysis Today. 2000;**63**:291-295. DOI: 10.1016/ S0920-5861(00)00471-5

[24] Chen Y, Zhang X, Dong M, Wu Y, Zheng G, Huang J, et al. MCM-41 immobilized 12-silicotungstic acid mesoporous materials: Structural and catalytic properties for esterification of levulinic acid and oleic acid. Journal of the Taiwan Institute of Chemical Engineers. 2016;**61**:147-155. DOI: 10.1016/j.jtice.2015.12.005

[25] Verpoort F. Materials Chemistry A. 2016. DOI: 10.1039/C6TA07860E

[26] Hartman BT, Brand R. Thesis for the degree of Master of Science In the Graduate School of Natural Sciences Debye Institute for Nanomaterials Science Inorganic Chemistry and Catalysis, (n.d.)

[27] Tari NE, Tadjarodi A, Tamnanloo J, Fatemi S. One pot microwave synthesis of MCM-41/Cu based MOF composite with improved CO_2 adsorption and selectivity. Microporous and Mesoporous Materials. 2016;**231**:154-162. DOI: 10.1016/j. micromeso.2016.05.027

[28] Bhatt AP, Pathak K, Jasra RV, Kureshy RI, Khan NUH, Abdi SHR. Chiral lanthanum-lithium-binaphthol complex covalently bonded to silica and MCM-41 for enantioselective nitroaldol (Henry) reaction. Journal of Molecular

13

Catalysis A: Chemical. 2006;**244**:110-117. DOI: 10.1016/j.molcata.2005.08.045

[29] Liu X, Luo J, Zhu Y, Yang Y, Yang S. Removal of methylene blue from aqueous solutions by an adsorbent based on metal-organic framework and polyoxometalate. Journal of Alloys and Compounds. 2015. DOI: 10.1016/j.jallcom.2015.07.065

[30] Lin S, Song Z, Che G, Ren A, Li P, Liu C, et al. Adsorption behavior of metal-organic frameworks for methylene blue from aqueous solution. Microporous and Mesoporous Materials. 2014. DOI: 10.1016/j.micromeso.2014.03.004

[31] Li L, Liu XL, Geng HY, Hu B, Song GW, Xu ZS. A MOF/graphite oxide hybrid (MOF: HKUST-1) material for the adsorption of methylene blue from aqueous solution. Journal of Materials Chemistry A. 2013. DOI: 10.1039/c3ta11478c